

Supplementary Materials

S1 Description of Hydrological Model

In the following the hydrological model structure and the underlying assumptions will be described and the corresponding equations provided.

The temperature lapse rate is set to $0.006 \text{ }^\circ\text{C m}^{-1}$ (e.g., Gao et al., 2014) to account for decreasing temperature with increasing elevation (see Eq. S1 where H_T defines the height at which temperature was measured (T_{meas}) and T_e the temperature at elevation H_e). A constant temperature lapse rate is assumed although in reality the lapse rate changes with season. However, a representation as a sine function of this seasonality does not improve model performance (Girons Lopez et al., 2020).

$$T_e = T_{meas} - 0.006 \cdot (H_e - H_T) \quad (\text{S1})$$

A threshold temperature (T_{thresh}) is employed to split precipitation into rain and snow. In the following two paragraphs the representation of interception and snow in the model is described. These two processes are run per elevation zone and the combined output of the elevation zones is used as input for the other processes in the model.

S1.1 Interception

The water stored in the interception reservoir (S_{int}) increases if precipitation is present as rain (P_{rain}) and decreases by interception evaporation (E_{int}) and outflow of water (P_{eff}) (Eq. S2).

The interception of precipitation by vegetation is represented as a threshold process because leaves can only hold a certain amount of water. If the interception capacity (I_{max}) is exceeded, excess water leaves the storage (P_{eff}) (Eq. S3). Afterwards water in the interception reservoir can evaporate (Eq. S4). The amount is limited by the water stored in the reservoir. Moreover, a limit of 50% of the potential evaporation is set to make the model more realistic. Thus, on cool humid days not all water potentially able to evaporate, evaporates from the interception storage but also soil evaporation can occur. Interception only takes place if temperature is above the threshold temperature which means precipitation enters the system as rain. For the bare rock HRU the process of interception is neglected as it is assumed to be negligible due to sparse vegetation.

$$\frac{dS_{int}}{dt} = P_{rain} - E_{int} - P_{eff} \quad (\text{S2})$$

$$P_{eff} = \max(S_{int} - I_{max}, 0) \cdot dt^{-1} \quad (\text{S3})$$

$$E_{int} = \min(0.5 \cdot E_{pot}, S_{int} \cdot dt^{-1}) \quad (\text{S4})$$

S1.2 Snow

The changes in the snow storage (S_{snow}) are represented by the input of snow (P_{snow}) if the temperature is below the threshold temperature and the output of melt water (M_{snow}) if temperature is above the threshold temperature (Eq. S5). The bare rock HRU also has a glacier storage ($S_{glacier}$, Eq. S6).

$$\frac{dS_{snow}}{dt} = P_{snow} - M_{snow} \quad (\text{S5})$$

$$\frac{dS_{glacier}}{dt} = P_{snow} - M_{glacier} \quad (S6)$$

The melt process which happens at temperatures above the threshold temperature is simulated with a degree-day approach. In this study it is assumed that the degree-day factor (DDF) (F_{melt}) is constant in time and space. Studies have shown that DDF increases during melt season, differs in different vegetation (Rango and Martinec, 1995), is correlated with elevation (He et al., 2014) and aspects of slopes. However, Griessinger et al. (2016) obtained similar results for a fixed DDF and a time-varying DDF for catchments with mean elevation below 2000m, Finger et al. (2015) showed that model performance does not increase with increasing complexity (including aspect or difference in vegetation) and Gao et al. (2017) show that including aspects does not improve the model performance but increases its spatial transferability. On the other hand, Abudu et al. (2016) illustrates that including aspects and slope slightly increased model performance. Girons Lopez et al. (2020) found a slight increase of model performance for a seasonal DDF. Yet, when evaluating increased model complexity against increased performance it was decided to implement a fixed DDF in order to keep the model simple. The melt process is represented by an exponential function as suggested by Girons Lopez et al. (2020) where M_M is the parameter to control for the smoothness of the snowmelt transition (Eq. S7) to increase the model performance. The process is limited by the amount of water stored in the snow reservoir (Eq. S8) whereas the process is unlimited for glaciers (Eq. S9). The threshold for melt was the same as the threshold for partitioning between rainfall and snow.

$$M = F_{melt} \cdot M_M \left(\frac{T - T_{thresh}}{M_M} + \ln(1 + \exp(-\frac{T - T_{thresh}}{M_M})) \right) \quad (S7)$$

$$M_{snow} = \min(M, S_{snow} \cdot dt^{-1}) \quad (S8)$$

$$M_{glacier} = M \quad (S9)$$

In the bare rock HRU, glaciers can exist, which are described as an unlimited reservoir. Glacial melting depends on the same DDF as snow melting (Eq. S9). Studies suggest a higher melt factor for glaciers than for snow (Braithwaite, 2008; He et al., 2014; Gao et al., 2017), because ice has a lower albedo than fresh snow which results in increased melting. However, glaciers are snow covered during a long period of the year. Thus, it was decided to use the same melt factor in order to not further increase the number of parameters. The total melt is the combination of snow and glacier melt according to the areal extent (Eq. S10).

$$M_{tot} = M_{snow} \cdot (1 - area_{gl}) + M_{glacier} \cdot area_{gl} \quad (S10)$$

The melt water is combined with the outflow of the interception reservoir over all elevation zones according to their areal extents.

$$P_{eff,tot} = \sum_{i=1}^{Elevations} P_{eff} + \sum_{i=1}^{Elevations} M_{tot} \quad (S11)$$

S1.3 Unsaturated Zone

The change in soil storage (S_u) is defined by the water entering the unsaturated zone (q_u) and the evaporation/transpiration of the soil (E_u).

$$\frac{dS_u}{dt} = q_u - E_u \quad (S12)$$

The amount of water entering the soil (q_u) is dependent on the water already stored in the reservoir and the maximum capacity of the soil storage (Eq. S13). The more water there is already stored in the reservoir, the less water will be stored. The relation is described by a monotonous increasing function for C_r (Eq. S14).

$$q_u = \min((1 - C_r) \cdot P_{eff,tot}, (S_{u,max} - S_u) \cdot dt^{-1}) \quad (\text{S13})$$

$$C_r = 1 - \left(1 - \frac{S_u}{S_{u,max}}\right)^\beta \quad (\text{S14})$$

The excess water is either diverted to the fast reservoir ($q_{overland}$) or reaches the slow reservoir as preferential flow (q_{pref}). The process is governed by the parameter ρ_p . Recharge into groundwater can occur on rainy days.

$$q_{overland} = (P_{eff,tot} - q_u) \cdot \rho_p \quad (\text{S15})$$

$$q_{pref} = (P_{eff,tot} - q_u) \cdot (1 - \rho_p) \quad (\text{S16})$$

$$S_u = S_u + q_u \cdot dt^{-1} \quad (\text{S17})$$

The transpiration of the unsaturated zone is only limited by the potential evaporation if the water stored in soil is greater than the proportion F_{evap} of $S_{u,max}$. Below, the flux is reduced linearly until reaching 0 for $S_u = 0$. The underlying reason is that the more water is stored in the soil the more water is stored in large pores, which plants can easier access. The less water stored, the more water is stored in small pores which cannot be fully used by the plants for transpiration.

$$E_u = (E_{pot} - E_{int}) \cdot \min\left(\frac{S_u}{S_{u,max} \cdot F_{evap}}, 1\right) \quad (\text{S18})$$

In the riparian HRU, water can also enter the soil from the slow reservoir via a flux q_{rip} (Eq. S20). The excess water flows into the fast reservoir (Eq. S21).

$$\frac{dS_{u,rip}}{dt} = q_{u,rip} - E_u \quad (\text{S19})$$

$$q_{u,rip} = \min((1 - C_r) \cdot (P_{eff,tot} + q_{rip}), (S_{u,max} - S_u) \cdot dt^{-1}) \quad (\text{S20})$$

$$q_{over} = P_{eff,tot} + q_{rip} - q_{u,rip} \quad (\text{S21})$$

S1.4 Fast Reservoir

The change in storage of the fast reservoir increases with water that does not enter the soil but runs off on the surface and decreases by runoff into the river (Eq. S22). It is expressed as a linear response reservoir with a reservoir constant (k_{fast}), so that each time step a fixed percentage of water is released into the river (Eq. S23).

$$\frac{dS_{fast}}{dt} = q_{overland} - q_{fast} \quad (\text{S22})$$

$$q_{fast} = k_{fast} \cdot S_{fast} \quad (\text{S23})$$

S1.5 Slow Reservoir

The change in slow reservoir is defined by the incoming preferential flow of all hillslope HRUs and the outflow q_{slow} (Eq. S24), which depends on the reservoir constant k_{slow} (Eq S25). Losses to deep ground water are neglected because it is assumed that the amount is so small that increasing the complexity of the model is not justified.

$$\frac{dS_{slow}}{dt} = q_{pref,bare} + q_{pref,forest} + q_{pref,grass} - q_{slow} \quad (S24)$$

$$q_{slow} = k_{slow} \cdot S_{slow} \quad (S25)$$

Part of the outflow q_{slow} enters the unsaturated zone of the riparian HRU, governed by the parameter ρ_{rip} (Eq. S26). The remaining water contributes to the river runoff (Eq. S27).

$$q_{rip} = \rho_{rip} \cdot q_{slow} \quad (S26)$$

$$q_{base} = (1 - \rho_{rip}) \cdot q_{slow} \quad (S27)$$

S1.6 River runoff

The river runoff at each time step is defined by the weighted sum of the outflows of the fast reservoirs of each HRU (q_{fast}) and the outflow of the slow reservoir (q_{base}).

$$Q_{river} = \sum_{i=1}^{HRU} q_{fast,i} + q_{base} \cdot (A_{bare} + A_{forest} + A_{grass}) \quad (S28)$$

A lag function to account for channel routing was not implemented in the model. The longest catchment (Gailtal) is 60 km long. Assuming a flow velocity of 1 m s^{-1} , it would take maximum 17 h for the water to get routed to the outlet of the catchment. As time steps of one day are used, channel routing can be neglected.

Loss Term Pitztal In the Pitztal water is diverted to a reservoir in the Kaunertal close by. The exact amount of water diversion at each time step is unknown but the maximum amount diverted is $12.1 \text{ m}^3 \text{ s}^{-1}$. It is assumed that during low runoff almost no water is diverted, whereas at high runoff the maximum amount is diverted. Thus, an exponential relationship with an upper boundary was assumed (Eq. S29). This results in an additional parameter that has to be calibrated ($loss$) which can range from 0.01 to 0.08.

$$Q_{loss} = \begin{cases} loss \cdot Q_{river}^2 & \text{if } loss \cdot Q_{river}^2 \leq 12.1 \\ 12.1 & \text{if } loss \cdot Q_{river}^2 > 12.1 \end{cases} \quad (S29)$$

$$Q_{river,real} = Q_{river} - Q_{loss} \quad (S30)$$

S2 Parameters

In order to reduce the number of parameters, most parameters are kept constant across HRUs. Only parameters for landscape dependent processes, i.e. interception and soil storage, are defined individually per HRU (see Table S1). Prior parameter ranges are determined based on literature (Gao et al., 2014; Prenner et al., 2018; Girons Lopez et al., 2020) and further improved based on first calibration runs in order to decrease the possible parameter space and improve calibration. To ensure parameter combinations of HRUs are in line with the perception of the system, they are constrained based on Gharari et al. (2014). The interception capacity of forest has to be larger than of grassland or of the riparian zone due to a higher Leaf Area Index of forests (Eq. S31 & S32). The soil storage capacity is constrained based on the assumption that larger plants have larger roots and a higher water demand and thus need more soil and a larger soil storage. Moreover, a larger soil storage capacity of grassland than riparian zone is assumed due to high ground water levels near the river shore (Eq. S33 & S34). Lastly, the reservoir constants were constrained by the rate at which they run off into the river (Eq. S35).

$$I_{max,forest} > I_{max,grass} \quad (S31)$$

$$I_{max,forest} > I_{max,rip} \quad (S32)$$

$$S_{u,max,forest} > S_{u,max,grass} > S_{u,max,rip} \quad (S33)$$

$$S_{u,max,forest} > S_{u,max,grass} > S_{u,max,bare} \quad (S34)$$

$$k_{fast,rip} > k_{fast} > k_{slow} \quad (S35)$$

S3 Objective Functions

In order to calibrate the model, it is necessary to compare the model output to runoff measurements based on so called objective functions. Due to high amount of parameters of the model it is necessary to use several objective functions to make sure that the model represents well the catchment behaviour. The overall performance of the model was assessed using the mean Euclidean Distance (D_e) from the perfect model fit (Hrachowitz et al., 2014).

Nash Sutcliffe efficiency A widely used objective function in hydrology is the Nash Sutcliffe Efficiency (NSE) (Eq. S36). The NSE ranges between 1 and $-\infty$. A perfect fit would result in a NSE of 1. A value of zero indicates that the mean observed stream flow is the best estimation of the model. The NSE tends to overemphasizes peak flows because the deviations between the model and observed stream flow are squared. Therefore, it is necessary to use another objective function which is focused on the low flows. A good objective function for this purpose is the Log Nash-Sutcliffe efficiency (Eq. S37) because it is more sensitive to low flows than to peak flows.

$$NSE = 1 - \frac{\sum_{i=1}^n (Q_{Mod,i} - Q_{Obs,i})^2}{\sum_{i=1}^n (Q_{Obs,i} - \overline{Q_{Obs}})^2} \quad (S36)$$

Table S1: Parameter range prior to calibration and 5th and 95th quantile of best parameter sets per catchment.

Global Parameters	Unit		Prior		Feistritz		Palten		Gaital		Silbertal		Defreggen		Pitztal	
	5 th	95 th														
T_{thresh}	°C	-2	2	-0.57	1.42	0.61	1.95	-0.1	1.33	0.93	1.97	1.77	2.48	1.8	2.49	
F_{melt}	mm/°C	1	6	1.3	4.58	1.87	3.89	1.06	1.99	1.7	2.88	2.25	4.18	2.08	3.84	
M_M	°C	0.001	1	0.05	0.95	0.05	0.93	0.05	0.96	0.05	0.93	0.03	0.9	0.05	0.93	
ρ_p	-	0.1	0.9	0.25	0.5	0.46	0.61	0.39	0.57	0.53	0.7	0.53	0.75	0.68	0.82	
k_{fast}	d ⁻¹	0.1	1	0.08	0.22	0.06	0.13	0.17	0.3	0.08	0.2	0.07	0.15	0.1	0.28	
k_{slow}	d ⁻¹	0.001	0.1	0.006	0.018	0.002	0.008	0.010	0.029	0.001	0.012	0.005	0.019	0.003	0.020	
F_{evap}	-	0.4	0.8	0.41	0.73	0.43	0.78	0.43	0.78	0.42	0.78	0.49	0.79	0.42	0.77	
Bare Rock																
$S_{u,max,bare}$	mm	1	50	2.68	46.68	2.38	43.57	2.01	44.43	3.1	45.8	1.87	47.28	9.58	48.23	
β_{bare}	-	0.1	2	0.21	1.89	0.19	1.91	0.24	1.9	0.21	1.93	0.26	1.95	0.37	1.82	
Forested Hillslope																
$I_{max,forest}$	mm	1	3	1.13	2.89	1.15	2.87	1.12	2.89	1.08	2.87	1.1	2.87	1.11	2.93	
$S_{u,max,forest}$	mm	50	500	65.32	144.82	61.31	366.04	57.15	308.74	83.3	389.73	94.87	380.1	88.07	473.46	
β_{forest}	-	0.1	2	0.18	0.9	0.21	1.95	0.13	1.78	0.27	1.9	0.36	1.94	0.18	1.91	
Grassland Hillslope																
$I_{max,grass}$	mm	1	2	0.13	1.86	0.07	1.83	0.09	1.82	0.06	1.76	0.06	1.74	0.06	1.78	
$S_{u,max,grass}$	mm	5	250	26.34	102.23	14.36	172.28	12.8	130.54	26.18	230.26	25.85	225.34	33.89	234.69	
β_{grass}	-	0.1	2	0.17	1.73	0.15	1.89	0.19	1.92	0.2	1.88	0.29	1.96	0.2	1.86	
Riparian Zone																
$I_{max,rip}$	mm	1	3	0.12	2.29	0.08	2.17	0.1	2.38	0.1	2.11	0.08	2.16	0.06	2.17	
$S_{u,max,rip}$	mm	5	250	8.69	73.68	6.06	117.77	6.4	76.05	8.61	164.71	9.44	161.58	9.13	156.96	
β_{rip}	-	0.1	2	0.18	1.85	0.19	1.84	0.21	1.9	0.27	1.9	0.19	1.94	0.19	1.87	
$K_{fast,rip}$	d ⁻¹	0.2	3	0.25	2.84	0.28	2.86	0.32	2.86	0.22	2.8	0.27	2.81	0.3	2.84	
ρ_{rip}	-	0.05	0.5	0.08	0.48	0.08	0.48	0.08	0.49	0.07	0.48	0.07	0.49	0.08	0.49	

$$NSE_{log} = 1 - \frac{\sum_{i=1}^n (\log(Q_{Mod,i}) - \log(Q_{Obs,i}))^2}{\sum_{i=1}^n (\log(Q_{Obs,i}) - \log(\overline{Q_{Obs}}))^2} \quad (S37)$$

Volumetric Efficiency The volumetric efficiency describes the fraction of water delivered at the proper time (Criss and Winston, 2008).

$$VE = 1 - \frac{\sum_{i=1}^n |Q_{Mod,i} - Q_{Obs,i}|}{\sum_{i=1}^n Q_{Obs,i}} \quad (S38)$$

Flow duration curve A Flow Duration Curve plots the magnitude of daily runoff against the exceedence probability on any day. The flow duration curve of the logarithmic flows is calculated. The NSE between the observed and modelled flow duration curve is taken as objective function. As the timing of the flow is not considered for FDC, but only the magnitude, this objective function focuses on the magnitude of flows, disregarding a proper representation of timing.

Autocorrelation The autocorrelation is a measure of the "memory" of the catchment. If the memory is high, the correlation values should be high and the hydrograph is smooth. If the memory is low, the correlation values are low and the hydrograph has sharp peaks. The autocorrelation with a lag of 1 day is calculated (see Eq. S39) and the results of observed and modelled streamflow are compared using the relative error. As another signature, the auto correlation values with a lag of 1 to 90 days are calculated. The resulting autocorrelation functions of the observed and modelled streamflow are compared using the NSE.

$$AC = \frac{\sum_{i=1}^n (Q_i - \overline{Q})(Q_{i+1} - \overline{Q})}{\sum_{i=1}^n (Q_i - \overline{Q})^2} \quad (S39)$$

Monthly runoff coefficient The runoff coefficient is the ratio of total runoff to total precipitation. If the monthly runoff coefficient are correctly represented by the model, it means that the model is able to reproduce the amount of runoff and evaporation correctly. The following function is used to calculate the monthly runoff with n the number of days in the corresponding month. The runoff coefficients of all months are compared using the NSE.

$$R = \frac{\sum_{i=1}^n Q}{\sum_{i=1}^n P} \quad (S40)$$

Snow cover Using satellite derived snow cover images for calibration significantly improves correct representation of glaciers, snow and rain (Finger et al., 2015). Thus, MODIS satellite data is used to determine the daily area fraction of the catchments covered by snow ($a_{obs,i}$) which is compared to the modeled area fraction covered by snow ($a_{mod,i}$), where an SC of one indicates a perfect fit.

$$SC = \frac{1}{n} \sum_{i=1}^n (1 - |a_{mod,i} - a_{obs,i}|) \quad (\text{S41})$$

S4 Calculation of analysis of change

S4.1 Timing of maximum/minimum flow

The mean timing of annual maximum and minimum flow over 30 years was calculated using the approach of circular statistics (e.g., Young et al., 2000; Blöschl et al., 2017). Therefore, the date of occurrence (D_i) has to be converted to an angle (Eq. S42) where $Lengyr$ denotes the number of days in each year. The date of occurrence for the annual maximum runoff is defined as the date of maximum daily runoff in a calendar year. The date of annual minimum flows is defined as the first day of the seven consecutive days with lowest flows in the time period from June to May.

$$\theta_i = D_i \cdot \frac{2\pi}{Lengyr_i} \quad (\text{S42})$$

The mean date of occurrence over the 30-year time period is calculated by

$$\bar{D} = \begin{cases} \tan^{-1}\left(\frac{\bar{y}}{\bar{x}}\right) \cdot \frac{Lengyr}{2\pi} & \bar{x} > 0, \bar{y} \geq 0 \\ (\tan^{-1}\left(\frac{\bar{y}}{\bar{x}}\right) + \pi) \cdot \frac{Lengyr}{2\pi} & \bar{x} \leq 0 \\ (\tan^{-1}\left(\frac{\bar{y}}{\bar{x}}\right) + 2\pi) \cdot \frac{Lengyr}{2\pi} & \bar{x} > 0, \bar{y} < 0 \end{cases} \quad (\text{S43})$$

using

$$\bar{x} = \frac{1}{n} \sum_{i=1}^n \cos \theta_i \quad (\text{S44})$$

$$\bar{y} = \frac{1}{n} \sum_{i=1}^n \sin \theta_i \quad (\text{S45})$$

$$\overline{Lengyr} = \frac{1}{n} \sum_{i=1}^n Lengyr_i \quad (\text{S46})$$

For calculating the distribution of the date of occurrences over the time period of 30 years, the year was divided into bins of 15 days, so 25 bins in total, with the last bin containing $DOY > 360$, so only 5 or 6 days. The fraction of occurrence per time bin was calculated as follows:

$$p_{15days} = \frac{\sum_{i=1}^{30} D_i}{30} \quad (\text{S47})$$

S4.2 Magnitude of annual maximum flow

In addition to calculating the mean magnitude of annual maximum flow, the distribution of magnitudes of annual maximum flow over 30 years was determined. Therefore, the magnitudes were ranked, from the highest ($i=1$) to lowest ($i=30$) annual maximum flow magnitude. The exceedance probability (p) was calculated, where N denotes the total number of observations, which is in this case 30.

$$p = \frac{i}{N + 1} \quad (\text{S48})$$

The return period (T_a) was calculated using the exceedance probability

$$T_a = \frac{1}{p} \quad (\text{S49})$$

The magnitudes in relation to the return periods were analysed by calculating the absolute and relative change of magnitude for each return period.

S5 Calibration & evaluation

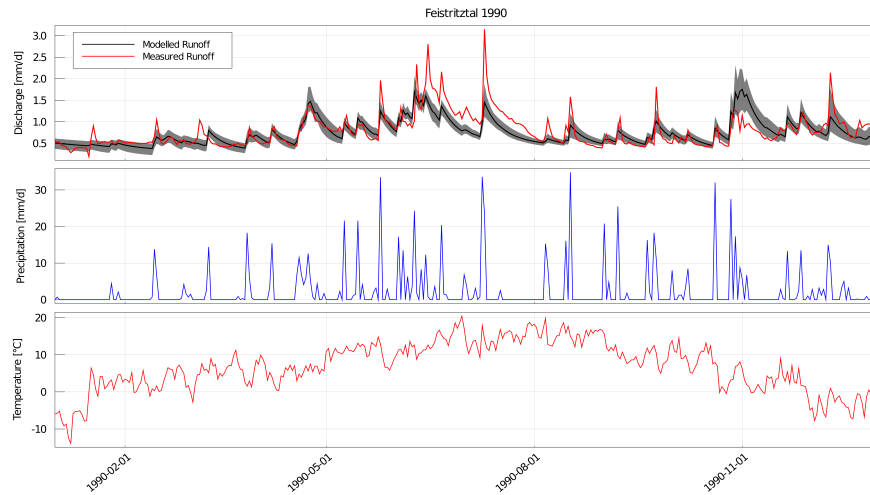


Figure S1: Feistritzal 1990: Comparison of measured and modelled runoff, also showing the corresponding precipitation and temperature, black line indicates mean modelled runoff using best parameter sets, shaded area shows the range of best parameter sets.

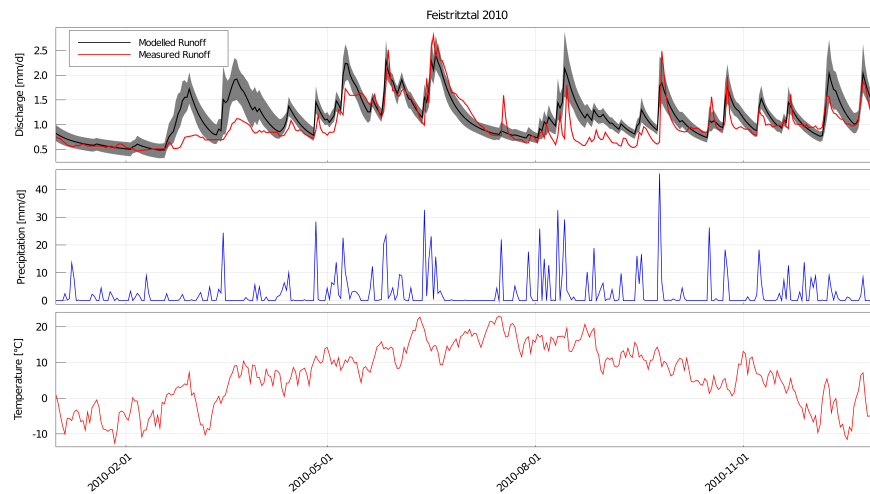


Figure S2: Feistritzal 2010: Comparison of measured and modelled runoff, also showing the corresponding precipitation and temperature, black line indicates mean modelled runoff using best parameter sets, shaded area shows the range of best parameter sets.

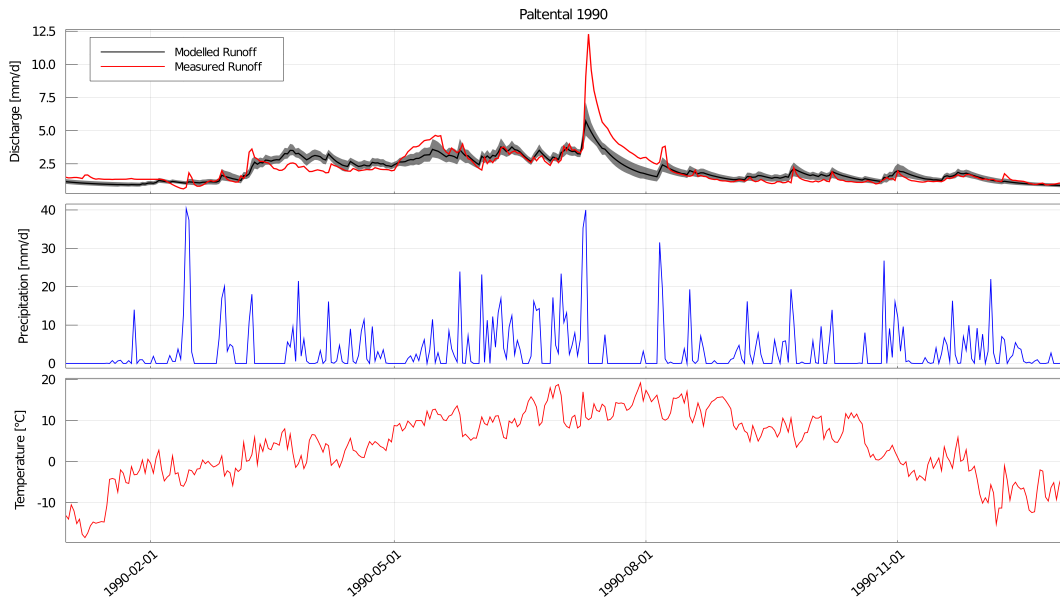


Figure S3: Paltental 1990: Comparison of measured and modelled runoff, also showing the corresponding precipitation and temperature, black line indicates mean modelled runoff using best parameter sets, shaded area shows the range of best parameter sets.

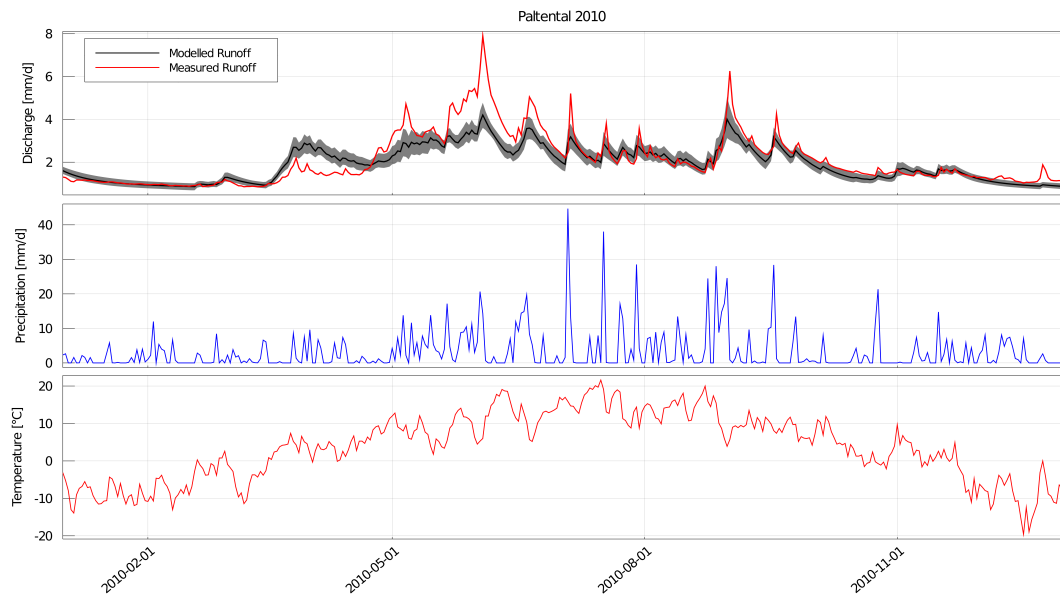


Figure S4: Paltental 2010: Comparison of measured and modelled runoff, also showing the corresponding precipitation and temperature, black line indicates mean modelled runoff using best parameter sets, shaded area shows the range of best parameter sets.

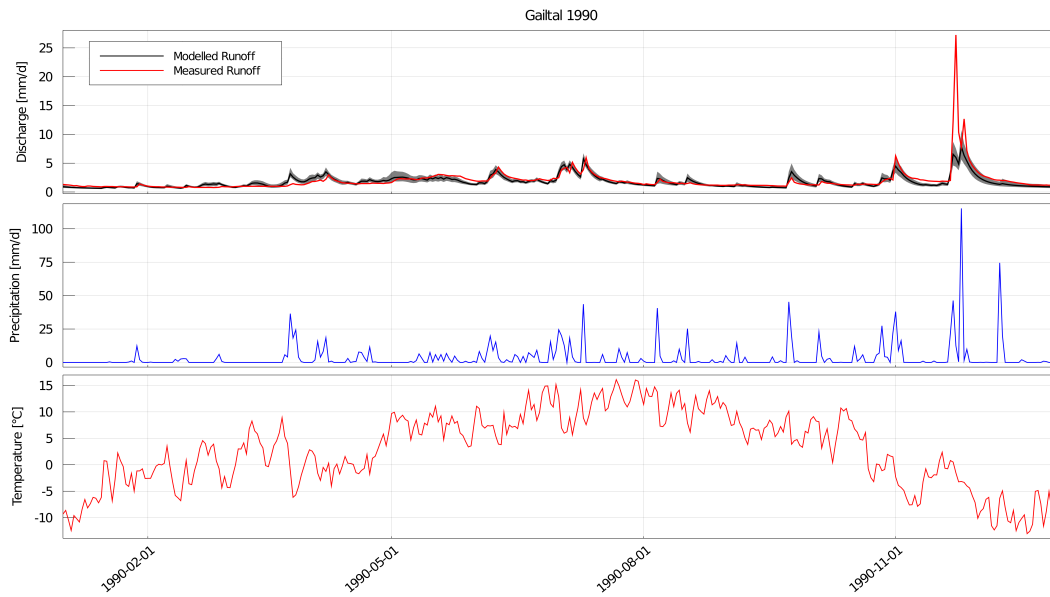


Figure S5: Gaital 1990: Comparison of measured and modelled runoff, also showing the corresponding precipitation and temperature, black line indicates mean modelled runoff using best parameter sets, shaded area shows the range of best parameter sets.

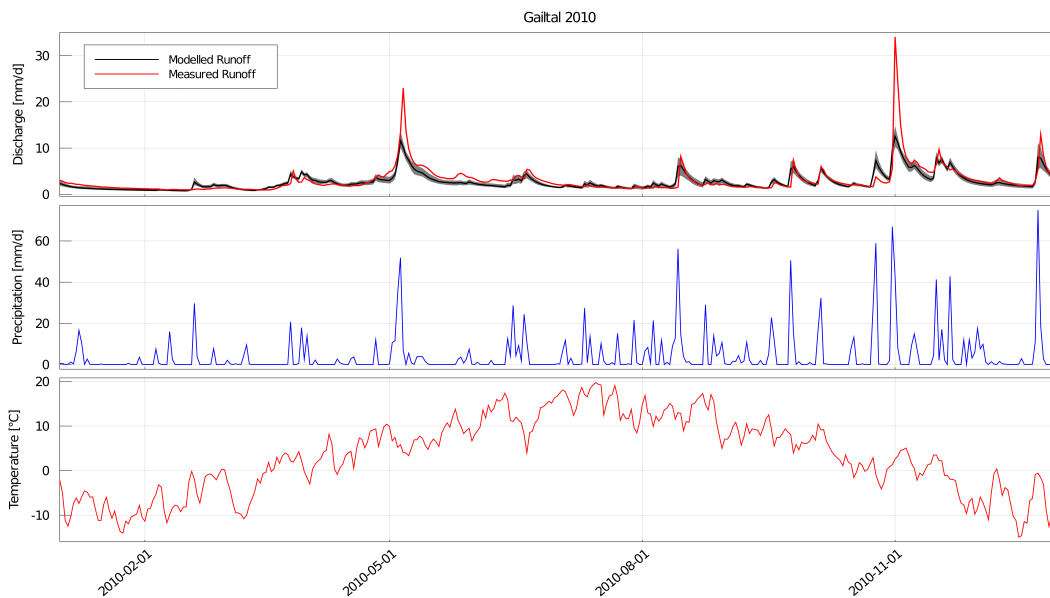


Figure S6: Gaital 2010: Comparison of measured and modelled runoff, also showing the corresponding precipitation and temperature, black line indicates mean modelled runoff using best parameter sets, shaded area shows the range of best parameter sets.

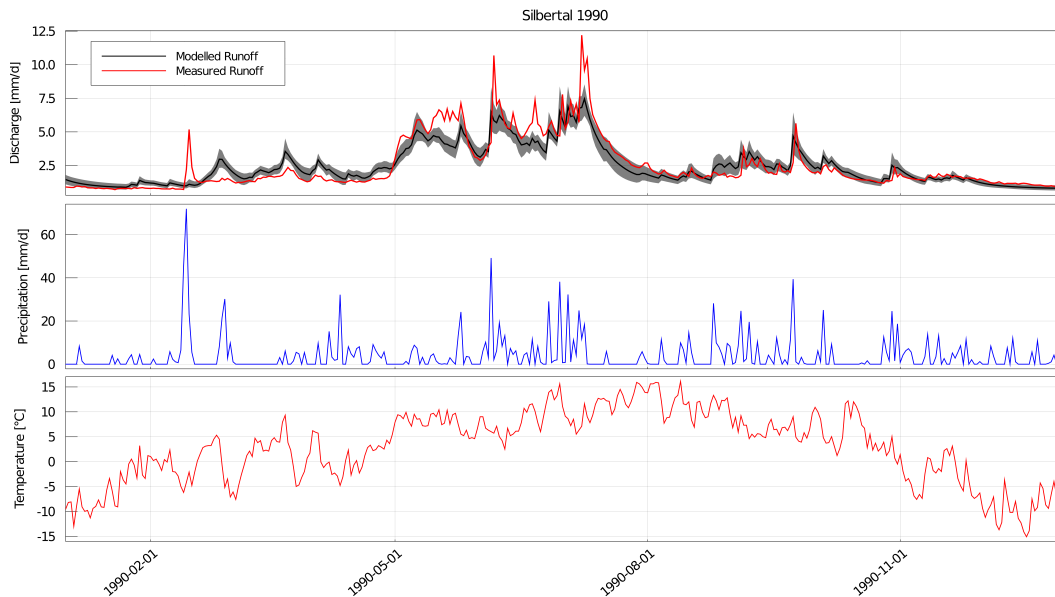


Figure S7: Silbertal 1990: Comparison of measured and modelled runoff, also showing the corresponding precipitation and temperature, black line indicates mean modelled runoff using best parameter sets, shaded area shows the range of best parameter sets, the measured runoff was scaled to match Budyko framework.

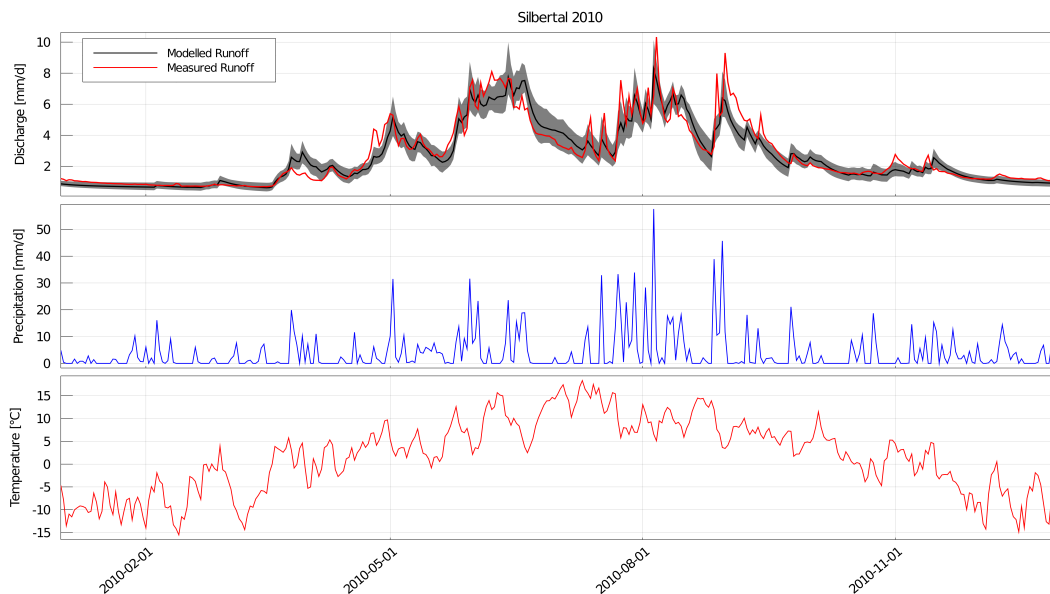


Figure S8: Silbertal 2010: Comparison of measured and modelled runoff, also showing the corresponding precipitation and temperature, black line indicates mean modelled runoff using best parameter sets, shaded area shows the range of best parameter sets, the measured runoff was scaled to match Budyko framework.

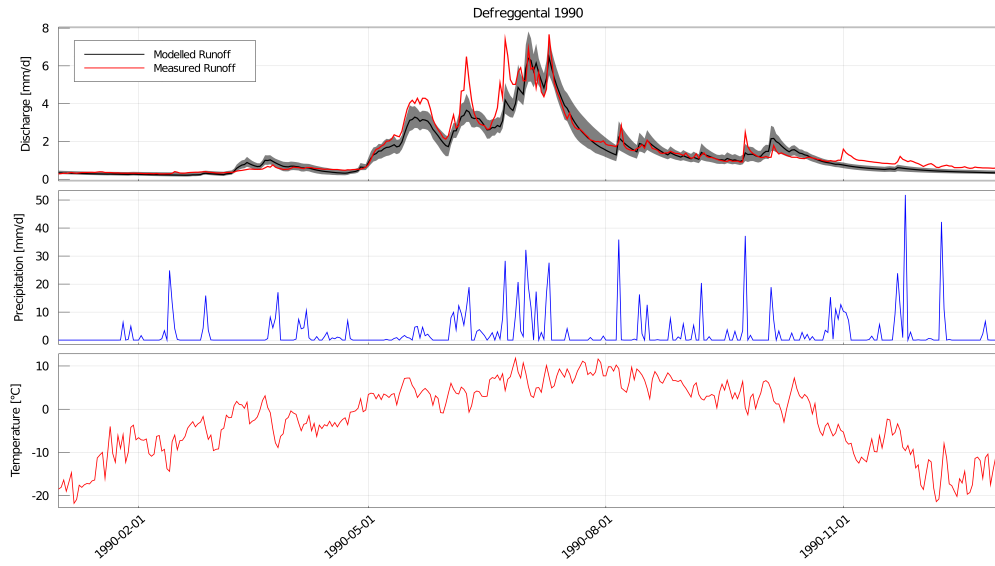


Figure S9: Defreggental 1990: Comparison of measured and modelled runoff, also showing the corresponding precipitation and temperature, black line indicates mean modelled runoff using best parameter sets, shaded area shows the range of best parameter sets, the measured runoff was scaled to match Budyko framework.

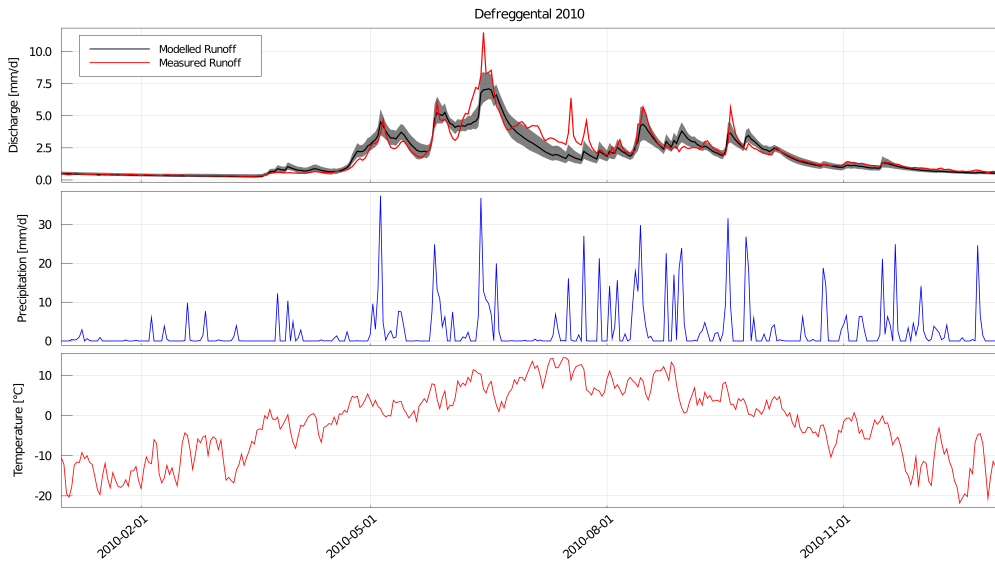


Figure S10: Defreggental 2010: Comparison of measured and modelled runoff, also showing the corresponding precipitation and temperature, black line indicates mean modelled runoff using best parameter sets, shaded area shows the range of best parameter sets, the measured runoff was scaled to match Budyko framework.

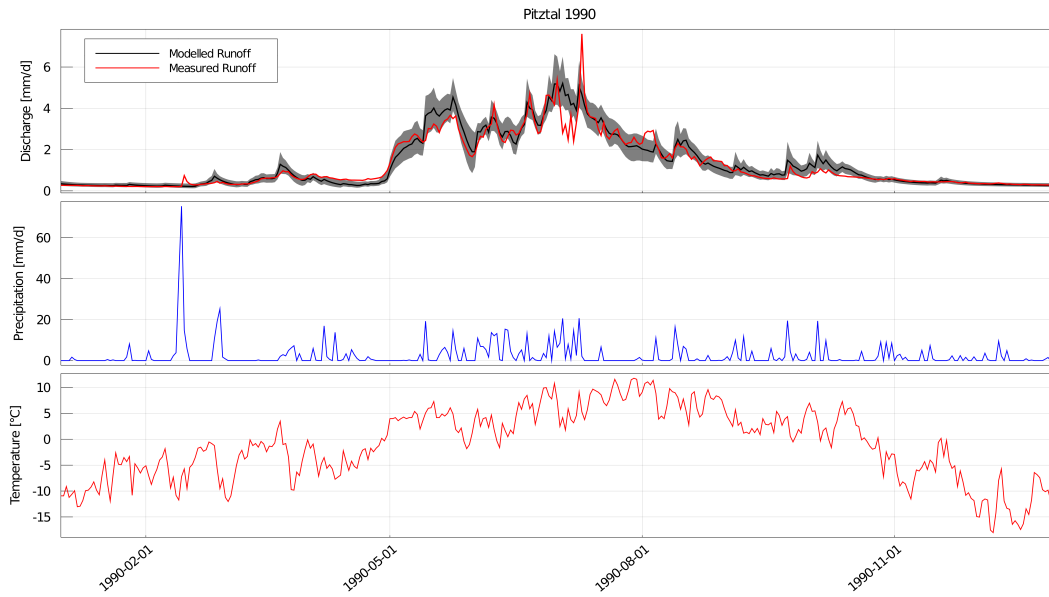


Figure S11: Pitztal 1990: Comparison of measured and modelled runoff, also showing the corresponding precipitation and temperature, black line indicates mean modelled runoff using best parameter sets, shaded area shows the range of best parameter sets.

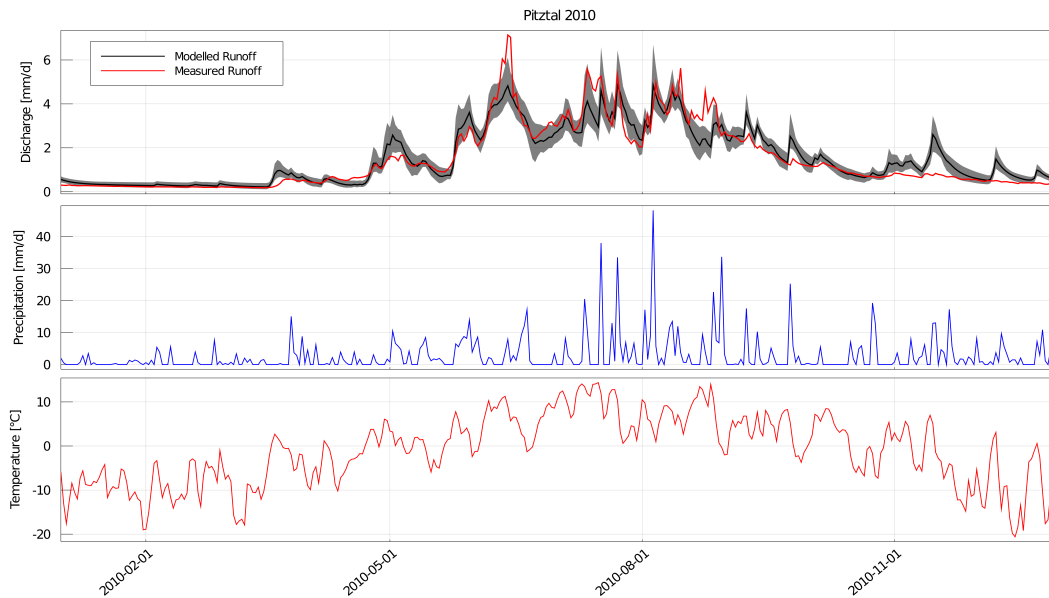


Figure S12: Pitztal 2010: Comparison of measured and modelled runoff, also showing the corresponding precipitation and temperature, black line indicates mean modelled runoff using best parameter sets, shaded area shows the range of best parameter sets.

S6 Measured data vs. climate simulations in the past

The following plots show the comparison of measured data and climate simulations for every catchment. Yearly extreme events, i.e. maximum precipitation, maximum/minimum runoff, are compared using empirical cumulative distribution functions (ECDF) to show the distribution of magnitudes and timing over a 22 to 30 year time period in the past, depending on the catchment. On the right, monthly temperature and precipitation of measured data (left) and climate simulations (right) are compared using boxplots. The lower right plot displays a comparison of mean monthly runoff over the time period using measured data as forcing for the hydrological model (left) or using climate simulations as forcing (right). The observed mean monthly runoff is also shown as a black X.

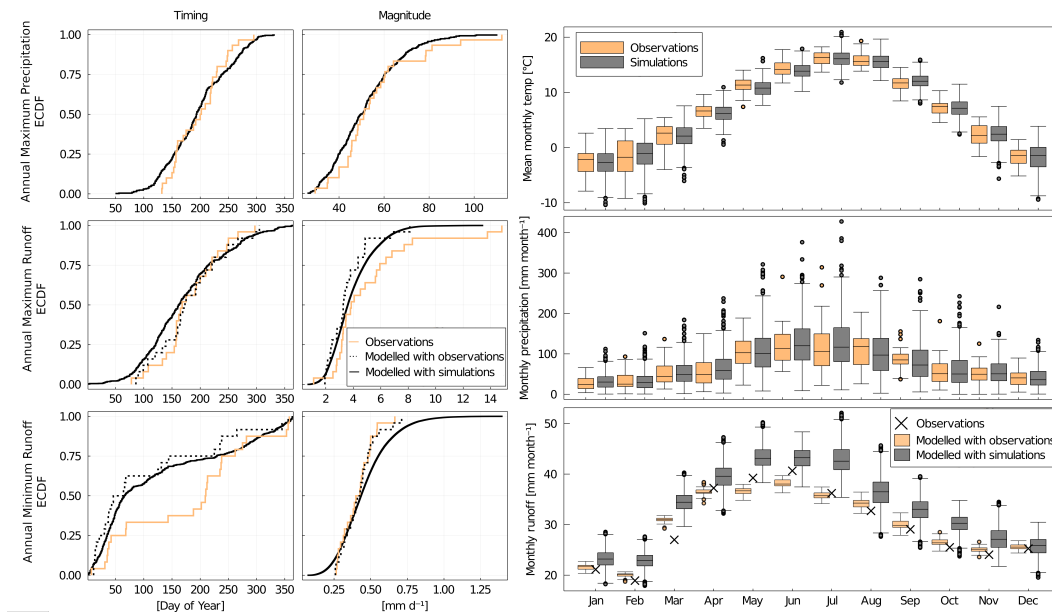


Figure S13: Comparison of measured data and climate simulations in the Feistritzal.

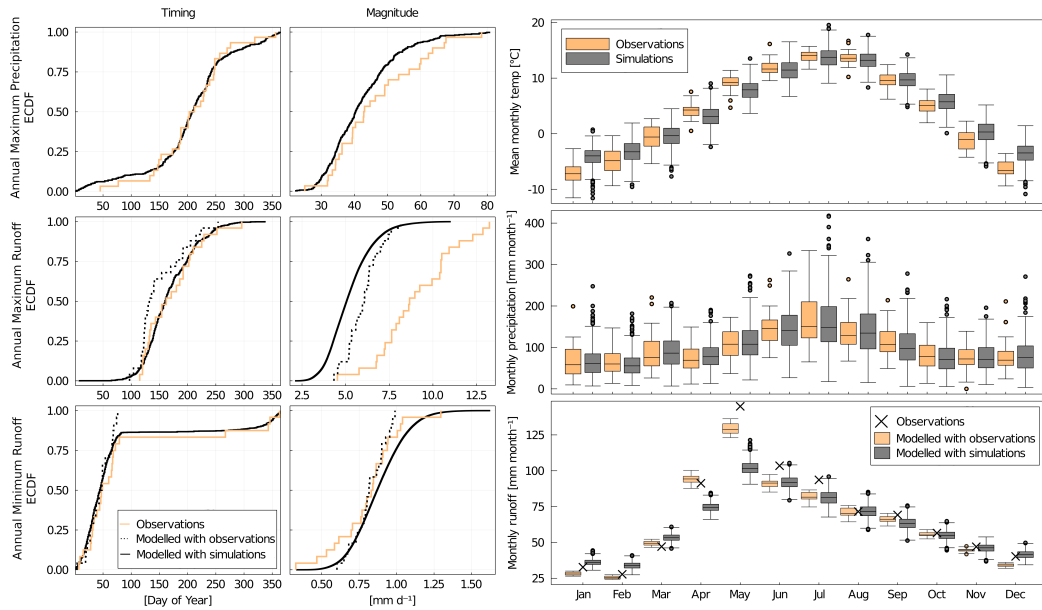


Figure S14: Comparison of measured data and climate simulations in the Paltental.

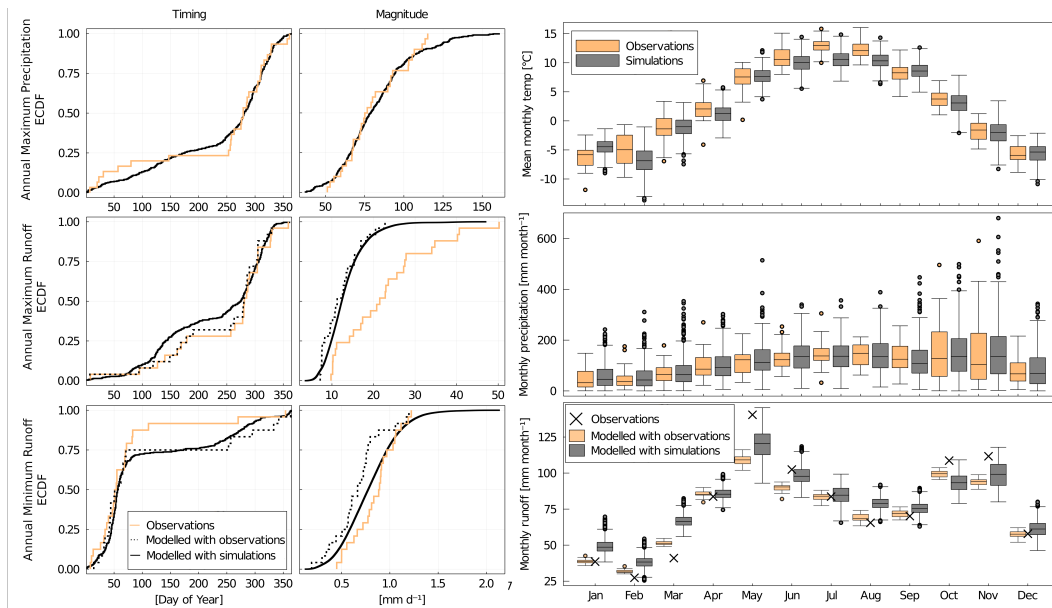


Figure S15: Comparison of measured data and climate simulations in the Gailtal.

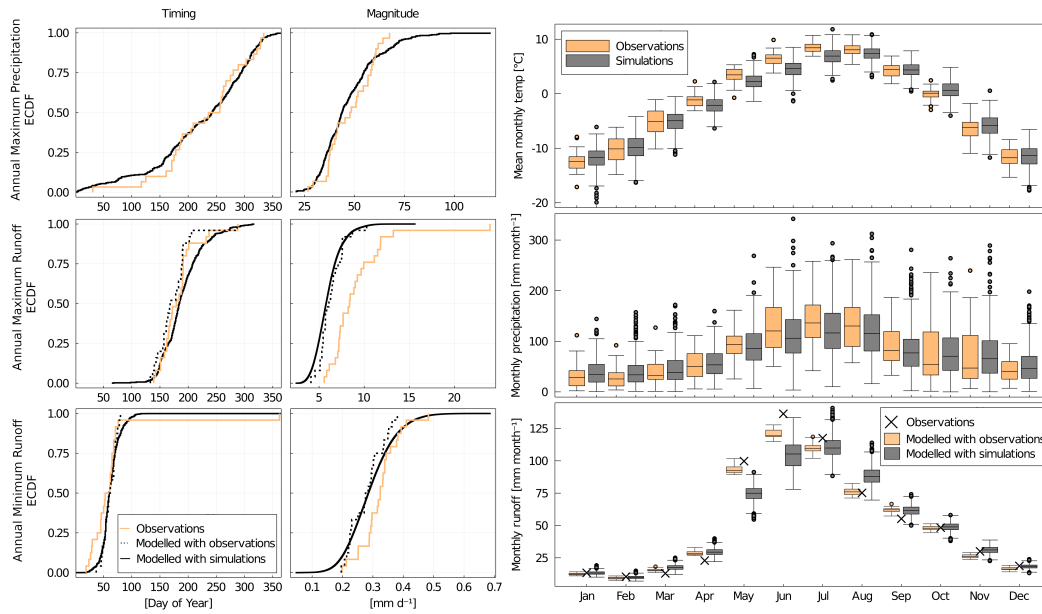


Figure S16: Comparison of measured data and climate simulations in the Defregental.

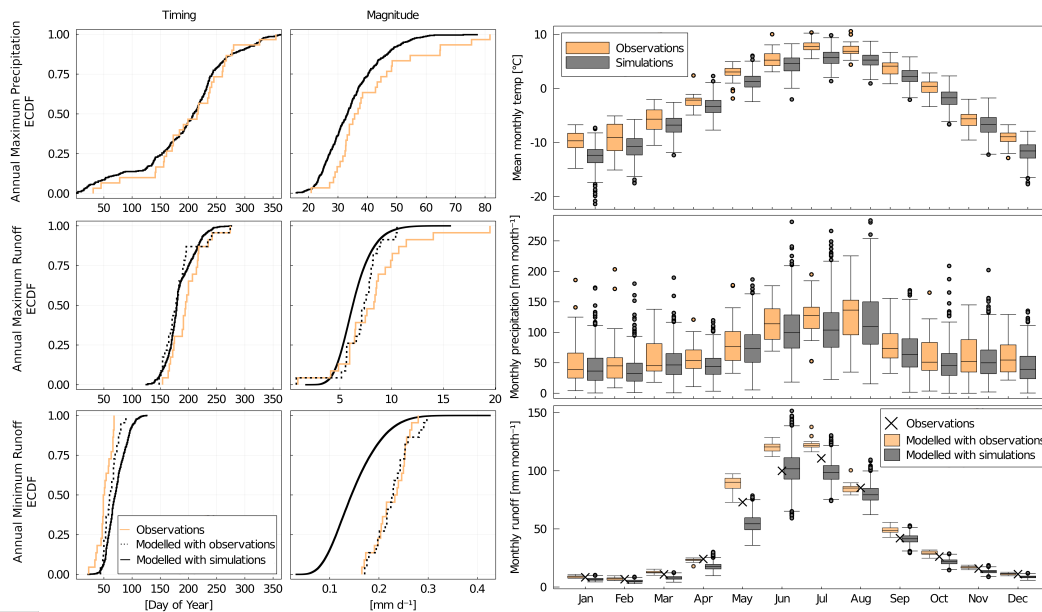


Figure S17: Comparison of measured data and climate simulations in the Pitztal.

S7 Additional figures

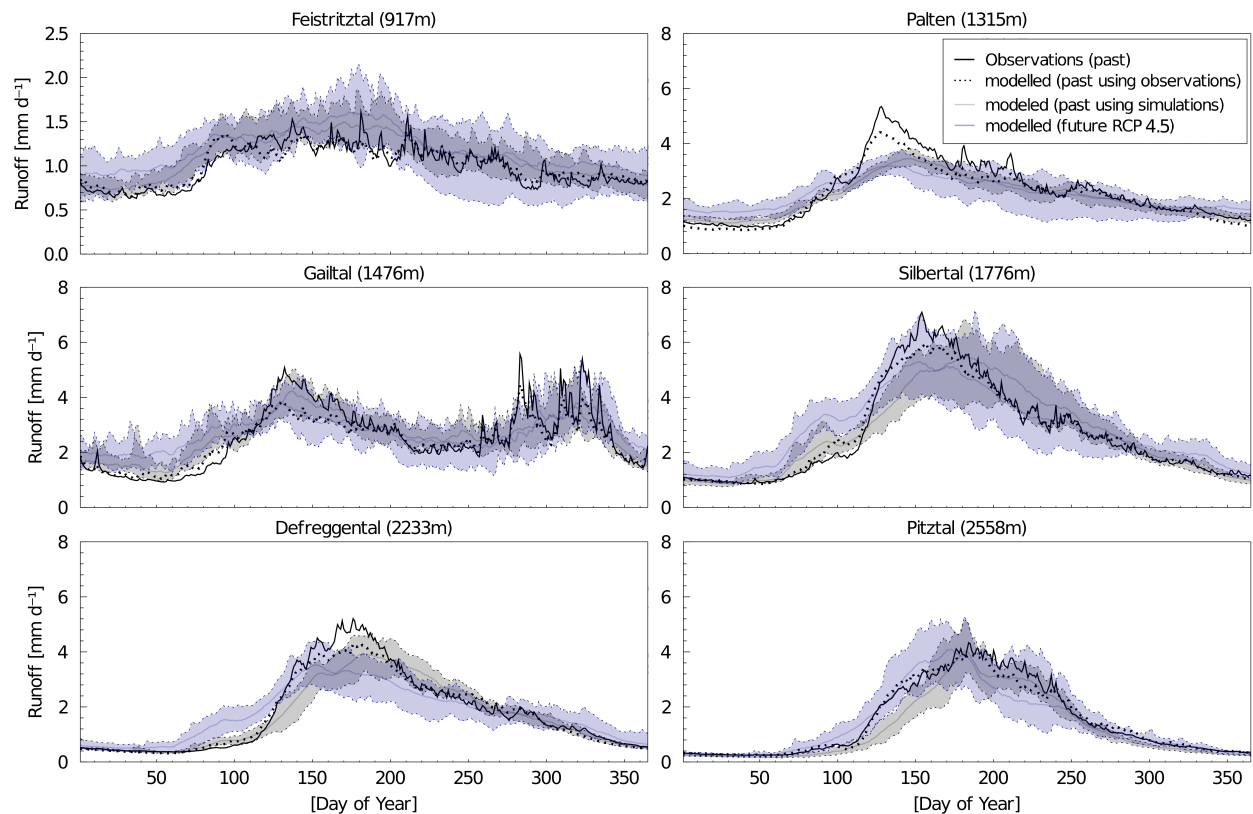


Figure S18: Comparison of observed (black line) and modelled runoff regime in past (1985–2013) using meteorological observations (dotted line) as well as runoff regimes modelled by climate simulations in past (1981–2010) and future (2071–2100) for RCP 4.5 (line represents the mean flow regime within the range of 14 climate models (shaded area)). Note that the extent of the y-axis differs for the Feistritzal.

References

- Abudu, S., Sheng, Z.-p., Cui, C.-l., Saydi, M., Sabzi, H.-Z., and King, J. P.: Integration of aspect and slope in snowmelt runoff modeling in a mountain watershed, *Water Science and Engineering*, 9, 265–273, URL <http://dx.doi.org/10.1016/j.wse.2016.07.002>, 2016.
- Blöschl, G., Hall, J., Parajka, J., Perdigão, R. A., Merz, B., Arheimer, B., Aronica, G. T., Bilibashi, A., Bonacci, O., Borga, M., et al.: Changing climate shifts timing of European floods, *Science*, 357, 588–590, 10.1126/science.aan2506, 2017.

- Braithwaite, R. J.: Temperature and precipitation climate at the equilibrium-line altitude of glaciers expressed by the degree-day factor for melting snow, *Journal of Glaciology*, 54, 437–444, 2008.
- Criss, R. E. and Winston, W. E.: Do Nash values have value? Discussion and alternate proposals, *Hydrological Processes*, 22, 2723–2725, 10.1002/hyp.7072, 2008.
- Finger, D., Vis, M., Huss, M., and Seibert, J.: The value of multiple data set calibration versus model complexity for improving the performance of hydrological models in mountain catchments, *Water Resources Research*, 51, 1939–1958, 10.1002/2014WR015712, 2015.
- Gao, H., Hrachowitz, M., Fenicia, F., Gharari, S., and Savenije, H.: Testing the realism of a topography-driven model (FLEX-Topo) in the nested catchments of the Upper Heihe, China, *Hydrology and Earth System Sciences*, 18, 1895, 10.5194/hess-18-1895-2014, 2014.
- Gao, H., Ding, Y., Zhao, Q., Hrachowitz, M., and Savenije, H. H.: The importance of aspect for modelling the hydrological response in a glacier catchment in Central Asia, *Hydrological Processes*, 31, 2842–2859, 10.1002/hyp.11224, 2017.
- Gharari, S., Hrachowitz, M., Fenicia, F., Gao, H., and Savenije, H.: Using expert knowledge to increase realism in environmental system models can dramatically reduce the need for calibration, *Hydrology and Earth System Sciences*, 18, 10.5194/hess-18-4839-2015, 2014.
- Girons Lopez, M., Vis, M. J., Jenicek, M., Griessinger, N., and Seibert, J.: Assessing the degree of detail of temperature-based snow routines for runoff modelling in mountainous areas in central Europe, *Hydrology and Earth System Sciences*, 24, 4441–4461, 10.5194/hess-24-4441-2020, 2020.
- Griessinger, N., Seibert, J., Magnusson, J., and Jonas, T.: Assessing the benefit of snow data assimilation for runoff modeling in Alpine catchments, *Hydrology and Earth System Sciences*, 20, 3895–3905, 10.5194/hess-20-3895-2016, 2016.
- He, Z., Parajka, J., Tian, F., and Blöschl, G.: Estimating degree day factors from MODIS for snowmelt runoff modeling, *Hydrology and Earth System Sciences*, 11, 10.5194/hess-18-4773-2014, 2014.
- Hrachowitz, M., Fovet, O., Ruiz, L., Euser, T., Gharari, S., Nijzink, R., Freer, J., Savenije, H., and Gascuel-Oudou, C.: Process consistency in models: The importance of system signatures, expert knowledge, and process complexity, *Water Resources Research*, 50, 7445–7469, 10.1002/2014WR015484, 2014.
- Prenner, D., Kaitna, R., Mostbauer, K., and Hrachowitz, M.: The value of using multiple hydrometeorological variables to predict temporal debris flow susceptibility in an alpine environment, *Water Resources Research*, 54, 6822–6843, 10.1029/2018WR022985, 2018.
- Rango, A. and Martinec, J.: Revisiting the degree-day method for snowmelt computations, *Water Resources Bulletin*, 31, 657–669, 1995.
- Young, A., Round, C., and Gustard, A.: Spatial and temporal variations in the occurrence of low flow events in the UK, *Hydrology and Earth System Sciences*, 4, 35–45, 2000.